Triple ionization of atomic Cd involving $4p^{-1}$ and $4s^{-1}$ inner-shell holes

J. Andersson,[1] R. Beerwerth,[2,3] P. Linusson,[4] J. H. D. Eland,[1,5] V. Zhaunerchyk,[1] S. Fritzsche,[2,3] and R. Feifel[1,6,*]

[1]*Department of Physics, University of Gothenburg, Origovägen 6B, SE-412 96 Gothenburg, Sweden*

[2]*Helmholtz-Institute Jena, D-07743 Jena, Germany*

[3]*Theoretisch-Physikalisches Institut, Friedrich-Schiller-Universität Jena, 07743 Jena, Germany*

[4]*Department of Physics, Stockholm University, AlbaNova University Center, SE-106 91 Stockholm, Sweden*

[5]*Department of Chemistry, Physical and Theoretical Chemistry Laboratory, Oxford University, South Parks Road, Oxford OX1 3QZ, United Kingdom*

[6]*Department of Physics and Astronomy, Uppsala University, Box 516, SE-751 20 Uppsala, Sweden*

(Received 2 July 2015; published 12 August 2015)

The triple ionization spectrum of atomic Cd formed upon the removal of a $4p$ or a $4s$ inner-shell electron and subsequent Auger decays has been obtained at 200 eV photon energy. By using a versatile multielectron coincidence detection technique based on a magnetic bottle spectrometer in combination with multiconfiguration Dirac-Fock calculations, Auger cascades leading to tricationic final states have been analyzed and final-state configurations have been identified. The most prominent Auger cascades leading to the ground state of Cd^{3+} have been identified in good agreement with theory.

DOI: 10.1103/PhysRevA.92.023414 PACS number(s): 33.80.Eh, 33.70.Ca, 34.50.Gb

I. INTRODUCTION

X-ray photoelectron spectroscopy (XPS) and Auger electron spectroscopy (AES) are both well-known analytical techniques used in many different research areas [1]. Auger-electron photoelectron coincidence spectroscopy combines the two techniques and can therefore serve for investigating in detail the energetic relations in Auger-electron cascades emitted by atoms, molecules, and solids. A highly efficient instrument for such studies is a magnetic bottle spectrometer [2], since it can detect essentially all electrons emitted into the solid angle of 4π, thereby making it possible to extract the correlation of multiple electrons and to obtain a wealth of information on multiple ionization events. In particular, by measuring the kinetic energies of all (or at least most) of the electrons emitted in multiple ionization events caused by initial single core hole formation, it is possible to analyze the final-state distributions and to get insight into the Auger cascade pathways leading to particular final states. Such analyses have already been performed for several rare gas atoms (see, e.g., Refs. [3–7]). However, there is still much work left to be done on exploring the energy correlations of electrons emitted by other atomic systems.

Since the first observation of an unusually broad feature in the conventional $4p$ photoelectron spectrum (PES) of Xe [8,9], which is explained by a breakdown of the independent particle model for the $4p^{-1}$ hole states due to rapid $4p^{-1} \rightarrow 4d^{-2}\epsilon f$ giant Coster-Kronig (GCK) transitions, it has become clear that this type of line broadening is not restricted to Xe. It has been concluded from XPS spectra of other systems that this peculiar spectral appearance extends to more elements of the periodic system close to Xe [8,10,11], especially to elements with atomic numbers between $46 \leqslant Z \leqslant 54$ [10]. For a review on this topic, see Ref. [12]. Cadmium with $Z = 48$ lies within this range and a $4p^{-1}$ hole can thus be expected to be strongly affected by very rapid $4p^{-1} \rightarrow 4d^{-2}\epsilon f$ GCK transitions causing an unusually broad feature ($\sim$25 eV) in the conventional electron spectra [10], as confirmed by previous spectroscopic studies of atomic Cd (e.g. [8]). Also a recent Auger-electron photoelectron coincidence spectroscopy study of doubly ionized Cd found that the $4p^{-1}$ hole states preferably decay in form of $4p^{-1} \rightarrow 4d^{-2}$ transitions [13]. In the same study, features in the double ionization spectra were observed at the binding energies 60–68 eV and were found to belong predominantly to the levels of the $4d^8nl,n'l'$ configurations [13].

In this work we present an extended Auger-electron photoelectron coincidence study on multiply ionized atomic Cd in combination with numerical calculations. We focus on triple ionization following the formation of $4p^{-1}$ and $4s^{-1}$ core holes with binding energies of 65–90 eV [8,10] and 115 eV [14], respectively. We study the associated final-state spectrum as well as effects of a $4p^{-1}$ hole either produced in the initial photoionization event or as part of a secondary Auger cascade.

II. EXPERIMENT

The experiments were carried out at beam line U49/2-PGM-2 of the BESSY-II storage ring in Berlin, Germany, in combination with a magnetic bottle multielectron coincidence spectrometer [2] for data collection. The storage ring provided light pulses of sub-ns widths, at a repetition rate of approximately 1.25 MHz. To reduce the pulse repetition rate to about 100 kHz, which is more suitable for our data aquisition system and which eliminates timewise overlapping coincidence events, a mechanical chopper synchronized to the storage ring has been used [15].

The principle of the magnetic bottle spectrometer has been described before [2]. Briefly, such an instrument collects essentially all electrons emitted in an ionization event at the light-matter interaction point by using the divergent field of a strong (ca. 1 T) permanent magnet to guide the electrons into a 2-m-long flight tube. The flight tube is provided with a comparatively weak axial solenoid field that confines the electrons on spiral trajectories towards a microchannel plate (MCP) detector. The measured quantity is the time of flight (TOF) of the electrons from the ionization point to the arrival at the detector. The TOFs are referenced to the synchrotron

*Corresponding author: raimund.feifel@physics.gu.se

radiation light pulses, and the corresponding kinetic energies are obtained by using a simple conversion formula, calibrated in the present study by examining the spectrum of known Xe-Auger lines [16].

The atomic vapor was produced by sublimating metallic Cd using a thermostatically controlled oven similar to the device used in Ref. [17]. The purity of the sample was verified by comparing measured single-electron spectra of Cd involving valence and core shells to known reference data [18]. In using 200 eV photon energy, the removal of either a $4p$ or a $4s$ electron, both with additional shakeup processes during the photoionization is possible. Since this is the same photon energy as previously used for analyzing the double ionization spectrum of Cd [13], the present study can be regarded as a direct extension of that previous work. In adjusting the radiation intensity to a level which implied low ionization event probability per light pulse, the present experimental data were obtained in classical coincidence conditions. This makes single, double, and triple ionization events distinguishable to the extent allowed by the ~50% collection-detection efficiency of the setup. It allows in particular the selection of individual electrons involved in the formation of a specific charge state and detailed extraction of their correlations with electrons of other kinetic energies.

III. THEORY

To better understand the results of this experiment and to support the data analysis, numerical calculations were performed. These included calculations of cross sections for the ionization of $4s$ and $4p$ electrons, starting from the $4d^{10}5s^2$ ground-state configuration of Cd. The resulting singly ionized states lie in the continuum of the next higher ionization stages and will preferably decay by autoionization.

We therefore also calculated the transition rates for an Auger decay of the $4s^{-1}$ and $4p^{-1}$ hole states to the possible final states of Cd^{2+}, where many of them will further decay radiatively towards the $4d^{10}$ ground state of this ion. However, some of these final states correspond to the $4p^{-1}5s^{-1}$ states or $4p^{-1}4d^{-1}$ and $4d^{-2}$ double hole state configurations that can autoionize again to the next higher charge state, Cd^{3+}. For this reason, we also calculated the transition rates for the second-step Auger decay to the possible states of triply ionized Cd^{3+}. From the calculated cross sections and transition rates, the branching ratios for the various decay paths leading to triply ionized states were derived and compared with the observed spectra.

The photoionization cross sections and the Auger transition rates are calculated by means of the RATIP toolkit [19]. The wave functions are generated by means of the multiconfiguration Dirac-Fock (MCDF) method, which is implemented in the GRASP code [20]. In the MCDF method, a wave function with given parity P, total angular momentum J, its projection J_z and a set of quantum numbers γ is represented as an expansion in so-called configuration state functions (CSFs) as

$$\Psi(\gamma,P,J,M)=\sum_{i=1}^{N}c_i(\gamma)\psi_i(\gamma_i,P,J,M). \qquad (1)$$

The configuration-state functions ψ_i are composed of orthonormal single-electron orbitals, and belong to an electronic configuration specified by the set of quantum numbers γ_i. The single-electron orbitals are calculated by means of a self-consistent optimization procedure using a relativistic Dirac Hamiltonian. The coefficients $c_i(\gamma)$ are computed by solving the eigenvalue problem of the Hamiltonian matrix, where additional relativistic effects are included by means of Breit interaction.

TABLE I. Electron configurations included in our calculations of the single-electron spectra. The number of levels for each electron configuration is also given.

Charge	Configuration	Levels
Cd	$4s^24p^64d^{10}\,5s^2$	1
Cd^{1+}	$4s\,4p^64d^{10}\,5s^2$	1
	$4s^2\,4p^54d^{10}\,5s\,6s$	7
	$4s^24p^54d^{10}\,5s^2$	2
Cd^{2+}	$4s^24p^54d^9\,5s^2$	12
	$4s^24p^54d^{10}\,5s$	4
	$4s^24p^64d^8\,5s\,6s$	32
	$4s^24p^64d^8\,5s^2$	9
	$4s^24p^64d^9\,6s$	4
	$4s^24p^64d^9\,5s$	4
	$4s^24p^64d^{10}$	1
Cd^{3+}	$4s^24p^64d^7\,5s^2$	19
	$4s^24p^64d^8\,5s$	16
	$4s^24p^64d^9$	2

In this work, we include all configurations that arise in the decay of the $4s^{-1}$ or $4p^{-1}$ hole state configurations. These configurations are listed in Table I. We found that Auger cascades leading to triply ionized final states are strongly influenced by shakeup transitions, where either the initial photoionization step or an Auger decay is accompanied by the excitation of a valence electron. In this case, a $5s$ electron is likely to be excited to a higher ns orbital, and therefore these configurations were also taken into account. Furthermore, shakeup transitions into the $5p$ shell are observed. To take these into account, we performed calculations including additional mixing with $5p^2$ and $5p$ configurations. That means we take virtual excitations of all $5s$ electrons to $5p$ orbitals into account, such that configurations like $4s^24p^54d^{10}5p^2$ and the triply ionized final state $4s^24p^64d^85p$ emerge.

A correct treatment of the shakeup transitions requires orbital relaxation due to the removal of inner-shell electrons to be taken into account. As a consequence, the orbitals of different ionization stages are not orthogonal to each other, which makes the computation of the atomic matrix elements more difficult. To account for that, we applied an approach based on the method of biorthonormal transformation [21]. In the following section, the corresponding numerical results are presented together with the experimental data.

IV. RESULTS

A. Cd^{3+} final-state spectrum

In Fig. 1 we present the experimental final-state spectrum of Cd^{3+} obtained at the photon energy of 200 eV. Here, triple

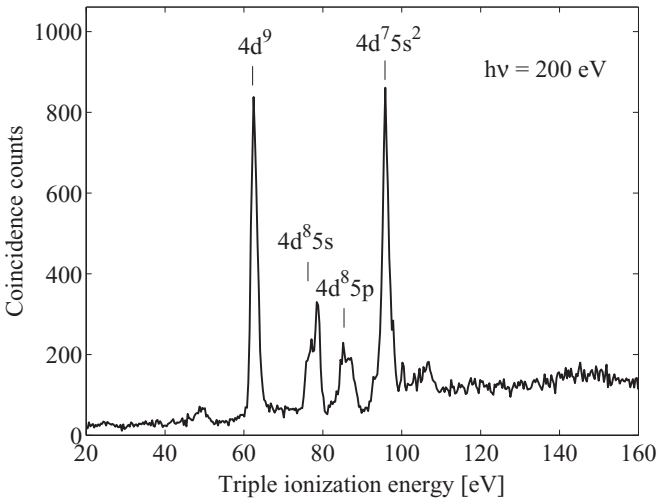

FIG. 1. Triple ionization spectrum of Cd produced mainly by the removal of either a $4p$ or $4s$ electron and subsequent Auger decay.

ionization energy (TIE) refers to

$$\mathrm{TIE} = h\nu - (\epsilon_1 + \epsilon_2 + \epsilon_3), \tag{2}$$

where $h\nu$ is the photon energy and the ϵ_i denote electron kinetic energies. The individual kinetic energies are obtained from the coincident measurement of the three electrons. We identify the strong peak at the triple ionization energy of about 63 eV as arising from the ground-state configuration $4d^9$ and the two peaks at around 78 and 85 eV as associated with the configurations $4d^8 5s$ and $4d^8 5p$, respectively. The above-mentioned peak positions are in good agreement with tabulated values available in the literature [18].

The assignment of the strong peak at about 96 eV needs more careful consideration. In this region, many states based on the configurations $4d^8 5d$, $4d^8 6s$, $4d^8 7s$, and $4d^7 5s^2$ can be expected. However, according to our numerical investigations, the high intensity can be understood primarily in terms of $4d^7 5s^2$ states, for reasons which will become clear below.

At about 106 eV a weak structure is observed which could correspond to $4d^8 4f$ or $4d^8 6p$ states [22] or to $4d^8 5f$ states, according to our calculations. In addition, the ns Rydberg series is expected to be energetically located in this region and could therefore contribute.

Furthermore, a weak peak at approximately 50 eV is observed. As the triple ionization energy of the ground state in Cd^{3+} is known to be around 63 eV [18], this peak must be regarded as an artifact, likely to be caused by accidental triple coincidences of electrons from the $4d^8 5s^2$ configuration in Cd^{2+} and a third stray electron.

The energy peak positions obtained from the final-state spectrum in Fig. 1 are summarized in the first column of Table II, and the relative peak intensities are included in the second column of this table. Since the resolution of the present experiment was not sufficiently high to resolve individual states of a certain configuration and since the majority of the peaks have an asymmetric profile, the positions were obtained as intensity weighted averages.

In order to investigate the tricationic states of Cd in further detail, we analyzed the coincidence map of Cd^{3+} in the form

TABLE II. Peak positions, relative intensities (integrated peak areas), and assignments of the final-state spectrum displayed in Fig. 1.

Position	Intensity (%)	Assignments
62.79	31.4	$4d^9$
77.63	15.8	$4d^8 5s$
85.73	12.8	$4d^8 5p$
96.35	36.5	$4d^7 5s^2$
105.69	3.5	
Total:	100	

where single-electron kinetic energies are plotted along the vertical axis and the triple ionization energy is plotted along the horizontal axis as presented in Fig. 2. In other words, this map shows single electrons detected in coincidence with particular final states and thereby gives important information on the formation of the tricationic states.

In projecting the data onto the (horizontal) triple ionization energy axis, one obtains the tricationic final-state spectrum of Cd discussed above, and in projecting the data onto the vertical axis, one obtains a single-electron spectrum that is reminiscent of a conventional electron spectrum of Cd. Since a photon energy of 200 eV was used for ionization, features corresponding to $4s^{-1}$ and $4p^{-1}$ core holes are primarily expected to be reflected along the vertical axis, where indeed a clear signal at about 85 eV kinetic energy and a broad signature between approximately 100–135 eV kinetic energy can be discerned. These structures are associated with the emission of $4s$ and $4p$ photoelectrons, respectively. The strong rise in single-electron signal towards low kinetic energy on the vertical axis is most likely caused by accidental coincidences involving stray electrons.

As can be seen from the map, triple ionization caused by $4p^{-1}$ hole formation predominantly decays to the ground-state configuration of Cd^{3+}, whereas the decay of the $4s^{-1}$ hole states gives more significant contributions to higher excited

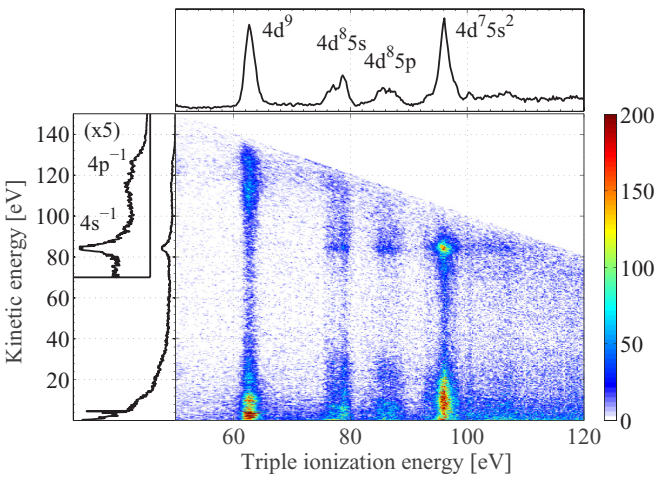

FIG. 2. (Color online) Coincidence map of single-electron energies (vertical axis) detected in coincidence with specific tricationic final states of atomic Cd (horizontal axis). One-dimensional spectra corresponding to intensity projections of the coincidence map onto the horizontal and vertical axes are included as well.

tricationic states, especially to the ones located at around 96 eV ionization energy. The ground-state signal is observed in coincidence with a strong Auger peak at about 5 eV and the 96 eV peak is observed in coincidence with electrons forming a broader island with a center at about 10 eV. A more detailed discussion of these features in Fig. 2 and on the formation of identified final states is given below.

B. $4d^9$ ground state of Cd^{3+}

Because the triple ionization energy of the Cd^{3+} ground state is less than the binding energy of a $4p^{-1}$ hole, it is energetically possible for both the $4p^{-1}$ and $4s^{-1}$ hole to lead to triple ionization. As can be seen in Fig. 2, the involvement of a $4s^{-1}$ hole in the formation of $4d^9$ states is hardly detectable. However, the broad signature at approximately 100–135 eV kinetic energy, associated with the emission of $4p$ photoelectrons, correlates strongly with production of the $4d^9$ configuration. We note that the island associated with $4p$ photoelectrons appears to have a tail toward lower kinetic energies, possibly obscuring the region of the $4s^{-1}$ feature. This comparatively long tail could be due to shakeup processes during the emission of $4p$ photoelectrons.

In order to identify the most prominent decay channels leading to the ground state of Cd^{3+} we applied the MCDF method described above for calculating Auger cascades. In all our calculations, we have neglected second- and higher-order processes, such as direct double ionization and direct double Auger decay. Within such a simplified consideration, the following four decay channels can lead to the formation of the ground state:

$$4s^{-1} \rightarrow 4p^{-1}4d^{-1} \rightarrow 4d^{-1}5s^{-2} \quad [4d^9] \tag{3}$$

$$4s^{-1} \rightarrow 4p^{-1}5s^{-1} \rightarrow 4d^{-1}5s^{-2} \quad [4d^9] \tag{4}$$

$$4s^{-1} \rightarrow 4d^{-2} \rightarrow 4d^{-1}5s^{-2} \quad [4d^9] \tag{5}$$

$$4p^{-1} \rightarrow 4d^{-2} \rightarrow 4d^{-1}5s^{-2} \quad [4d^9] \tag{6}$$

Our calculations suggest that channels (3) to (5) do not practically occur as almost all $4s^{-1}$ hole states decay to the $4d^7 5s^2$ configuration. Furthermore, a large fraction of the $4p^{-1}$ hole states were observed in the study on Cd^{2+} to decay to the $4d^8 5s^2$ configuration; cf. Ref. [13]. However, since the energy of all $4d^8 5s^2$ states is below the ground-state energy of Cd^{3+}, channel (6) can also be excluded. Our calculations also showed that some $4d^8 5s6s$ states have energies above the ground state energy of Cd^{3+}, which agrees with previous findings in the study on double ionization [13]. We therefore also included several shakeup transitions in our computations, as discussed in following subsection.

1. *Auger cascades with $5s \rightarrow (6s + 7s)$ shakeup transitions*

In principle, shake transitions can occur both during the initial photoionization process and in the subsequent Auger decay. We therefore included the following two decay channels leading to the ground state of Cd^{3+}:

$$4p^{-1} \rightarrow 4d^{-2}5s^{-1}6s \rightarrow 4d^{-1}5s^{-2} \quad [4d^9] \tag{7}$$

$$4p^{-1}5s^{-1}6s \rightarrow 4d^{-2}5s^{-1}6s \rightarrow 4d^{-1}5s^{-2} \quad [4d^9] \tag{8}$$

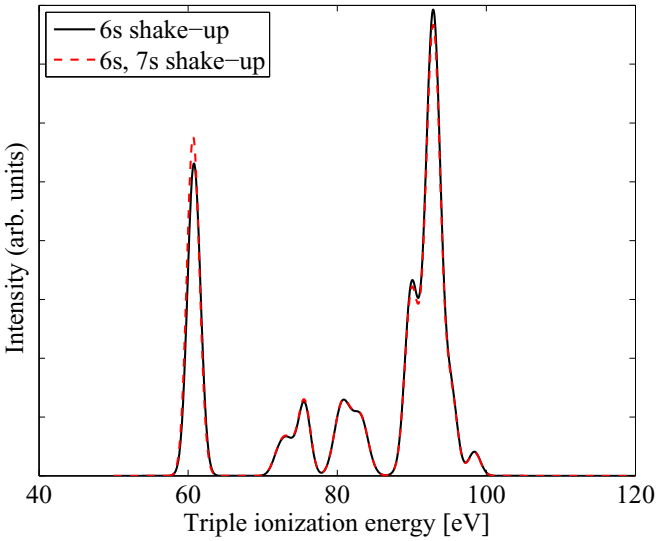

FIG. 3. (Color online) Theoretical final-state spectrum of Cd^{3+}. The four peak structures seen correspond to the $4d^9$ ground-state configuration, and the $4d^8 5s$, the $4d^8 5p$ as well as the $4d^7 5s^2$ excited-state configurations. (a) Calculated spectrum (solid line) by considering single ionization transitions as well as $5s \rightarrow 6s$ shakeup transitions. (b) Spectrum (red, dashed line) calculated similar to (a) but where $5s \rightarrow 7s$ shakeup transitions were included in the calculations. The latter leads to a change in the relative intensities of the peaks where the ground state got somewhat increased.

where sequence (7) corresponds to a $5s \rightarrow 6s$ shakeup during the GCK transition and sequence (8) to a $5s \rightarrow 6s$ shakeup during the initial photoionization step.

Figure 3 shows the calculated relative intensity of the electron emission as function of the triple ionization energy of Cd^{3+}. The black solid line in this figure presents the calculated final-state spectrum of Cd^{3+} where the decay channels (3)–(8) were taken into account. In addition, all decay channels between the configurations listed in Table I that lead to the identified excited Cd^{3+} states have been taken into account. All $5s \rightarrow ns$ shakeup transitions associated with $4s^{-1}$ holes were neglected due to computational restrictions. Shakeup transitions leading to $4d^8 5p$ states have been considered by means of configuration mixing between $5s^2$ and $5p^2$. In comparison to the experimental spectrum shown in Fig. 1, we see that the ratio between the two strongest peaks differs, an aspect which we will return to in the next section.

To further understand the importance of shakeup transitions, we also included shakeup transitions involving the $7s$ orbital. The two channels

$$4p^{-1} \rightarrow 4d^{-2}5s^{-1}7s \rightarrow 4d^{-1}5s^{-2} \quad [4d^9] \tag{9}$$

$$4p^{-1}5s^{-1}7s \rightarrow 4d^{-2}5s^{-1}7s \rightarrow 4d^{-1}5s^{-2} \quad [4d^9] \tag{10}$$

were therefore also taken into account in addition to channel (7) and (8). The corresponding spectrum is displayed with a red dashed line in Fig. 3. This spectrum is very similar to the $6s$ shakeup spectrum, apart from the ratio between the peaks which reflect the ground state and the $4d^7 5s^2$ states somewhat decreased.

2. *Comparison with experimental results*

In comparing the theoretical final-state spectra in Fig. 3 with the experimental spectrum displayed in Figs. 1 and 2 we note that the intensity ratio between the peak structure associated with the $4d^7 5s^2$ configuration and the ground state is still too high. The intensity ratio decreased when we included the additional $5s \rightarrow 7s$ shakeup transitions as new decay channels were opened up. These channels compete with decay channels of the $4s^{-1}$ hole and therefore reduce the intensity of the $4d^7 5s^2$ final-state configuration. Another reason for the shortcoming could be that the levels possibly contributing to the small peak structure at about 106 eV were not included in the calculations. As these levels are populated through decays of $4s^{-1}$ holes, similarly to the $4d^7 5s^2$ peak, neglecting them leads to an overestimation of the intensity of the $4d^7 5s^2$ peak.

In Fig. 4 we compare the experimental and theoretical single-electron spectra of transitions forming ground-state Cd^{3+} ions. The theoretical spectrum was obtained in a calculation separate from the ones of the overall final-state spectrum. The peaks are numbered and the strongest associated decay channels identified by our calculations are given in Table III. The previously explained shakeup transitions into the $6s$ and $7s$ shells are taken into account. Due to computational restrictions, our energy levels have an uncertainty of about 5%–10%. Some energies were therefore shifted to compensate for this uncertainty and to match the experimental results better. As the three ionization energies are in rather good agreement with the experimental data, the energies of Cd and Cd^{3+} states were not changed. The energies of Cd^+ states were shifted to match the energy of the $4s^{-1}$ hole to the experimental value and the energies of Cd^{2+} states were shifted to match the second strongest Auger peak to its experimental position. Our limited precision regarding energy levels is then reflected in the discrepancy between calculated and measured peak energies.

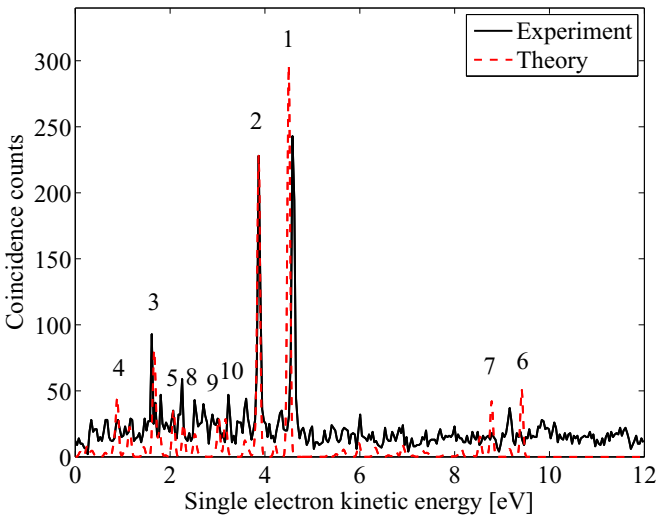

FIG. 4. (Color online) Comparison of the calculated and measured single-electron spectra. Peak numbers are used to label the transitions listed in Table III which are schematically illustrated in the level diagram displayed in Fig. 5.

However, the overall agreement is good considering the low signal-to-noise ratio of most of the experimental peaks.

C. $4d^8 5s$ and $4d^8 5p$ excited states of Cd^{3+}

From the coincidence map displayed in Fig. 2 we can see that both the $4d^8 5s$ and $4d^8 5p$ states are populated primarily by decay of a $4s^{-1}$ hole, although contributions from $4p^{-1}$ photoelectron shakeup states cannot be excluded. The comparatively limited statistics for these two final states makes a detailed analysis of the involved decay pathways more difficult. We will therefore give only a short qualitative interpretation of the possible decay paths involved.

In Cd, a $4s^{-1}$ hole is expected to most dominantly decay through a $4s^{-1} \rightarrow 4p^{-1}4d^{-1}$ super Coster-Kronig (SCK) transition [12]. If this is true, a possible decay path leading to the $4d^8 5s$ configuration could be the

$$4s^{-1} \rightarrow 4p^{-1}4d^{-1} \rightarrow 4d^{-2}5s^{-1} \tag{11}$$

transitions with an additional $5s \rightarrow 5p$ Auger shakeup in one of the steps when leading to $4d^8 5p$. However, the decay route

$$4s^{-1} \rightarrow 4p^{-1}5s^{-1} \rightarrow 4d^{-2}5s^{-1} \tag{12}$$

with additional $5s \rightarrow 5p$ Auger shakeup for the formation of the $4d^8 5p$ configuration is also possible. In principle, similar shakeup transitions could also occur during the initial $4s$ photoionization step, but as no clear signature of such events are present in the coincidence map (cf. Fig. 2), it seems less important. Because pathways (11) and (12) include creation and annihilation of a $4p^{-1}$ vacancy, both the first and second Auger electron is expected to have a broad kinetic-energy distribution. We note that although it is difficult to distinguish two broad Auger peaks from the noise level in our data, narrow Auger peaks do not seem to be present.

D. $4d^7 5s^2$ excited states of Cd^{3+}

From Fig. 2, we see that the most intense $4s$ photoelectron island appears in coincidence with the final state peak at ~96 eV. It also appears that this island has a tail on the low kinetic-energy side along the vertical axis which indicates that shakeups caused during the photoionization step could be present. In addition, the $4s$ photoelectrons forming the ~96 eV peak were observed in coincidence with the electrons associated with the broad feature at about 10 eV in Fig. 2.

As mentioned above, the majority of the $4s^{-1}$ hole states are expected to decay through $4s^{-1} \rightarrow 4p^{-1}4d^{-1}$ SCK transitions which could be likely candidates for explaining the 96 eV structure in the coincidence map. In constructing a double ionization spectrum based on the $4s^{-1}$ photoelectrons measured in coincidence with an additional electron from the broad island at ~10 eV, we observe a strong broad feature in the ionization energy range of about 96–115 eV. This coincides with the expected binding energy of the $4p^{-1}4d^{-1}$ multiplet. The same feature was already observed in the double ionization work on Cd (Fig. 5 in Ref. [13]), where it was mentioned that the $4p^{-1}4d^{-1}$ states are likely to decay very rapidly in the form of $4p^{-1}4d^{-1} \rightarrow 4d^{-3}$ GCK transitions (see Refs. [23,24]). Because the $4p^{-1}4d^{-1}$ states are primarily expected to decay in the form of $4p^{-1}4d^{-1} \rightarrow 4d^{-3}$ GCK transitions, we assume

TABLE III. Strongest decay channels leading to the ground state of Cd^{3+}. The first column contains the numbers used for labeling the features observed in Fig. 4 and schematically explained in Fig. 5.

Number	Cd^{1+}	Cd^{2+}	Cd^{3+}	Kin. energy (eV)
1	$4p^5 4d^{10}\,5s\,6s\,(^2P_{3/2})$	$4d^8\,5s\,6s\,(^1G_4)$	$4d^9\,(^2D_{5/2})$	4.49
2	$4p^5 4d^{10}\,5s\,6s\,(^2P_{3/2})$	$4d^8\,5s\,6s\,(^1G_4)$	$4d^9\,(^2D_{3/2})$	3.86
1	$4p^5 4d^{10}\,5s\,6s\,(^2P_{1/2})$	$4d^8\,5s\,6s\,(^1G_4)$	$4d^9\,(^2D_{5/2})$	4.49
2	$4p^5 4d^{10}\,5s\,6s\,(^2P_{1/2})$	$4d^8\,5s\,6s\,(^1G_4)$	$4d^9\,(^2D_{3/2})$	3.86
1	$4p^5 4d^{10}\,5s^2\,(^2P_{3/2})$	$4d^8\,5s\,6s\,(^1G_4)$	$4d^9\,(^2D_{5/2})$	4.49
3	$4p^5 4d^{10}\,5s\,6s\,(^2P_{3/2})$	$4d^8\,5s\,6s\,(^3F_4)$	$4d^9\,(^2D_{5/2})$	1.66
2	$4p^5 4d^{10}\,5s^2\,(^2P_{3/2})$	$4d^8\,5s\,6s\,(^1G_4)$	$4d^9\,(^2D_{3/2})$	3.86
4	$4p^5 4d^{10}\,5s\,6s\,(^2P_{3/2})$	$4d^8\,5s\,6s\,(^3F_4)$	$4d^9\,(^2D_{5/2})$	0.87
1	$4p^5 4d^{10}\,5s^2\,(^2P_{1/2})$	$4d^8\,5s\,6s\,(^1G_4)$	$4d^9\,(^2D_{5/2})$	4.49
2	$4p^5 4d^{10}\,5s^2\,(^2P_{1/2})$	$4d^8\,5s\,6s\,(^1G_4)$	$4d^9\,(^2D_{3/2})$	3.86
5	$4p^5 4d^{10}\,5s\,6s\,(^2P_{3/2})$	$4d^8\,5s\,6s\,(^3F_3)$	$4d^9\,(^2D_{5/2})$	2.06
6	$4p^5 4d^{10}\,5s\,6s\,(^2P_{3/2})$	$4d^8\,5s\,7s\,(^1G_4)$	$4d^9\,(^2D_{5/2})$	9.40
8	$4p^5 4d^{10}\,5s\,6s\,(^2P_{3/2})$	$4d^8\,5s\,6s\,(^3F_2)$	$4d^9\,(^2D_{5/2})$	2.27
3	$4p^5 4d^{10}\,5s^2\,(^2P_{3/2})$	$4d^8\,5s\,6s\,(^3F_4)$	$4d^9\,(^2D_{5/2})$	1.66
7	$4p^5 4d^{10}\,5s\,6s\,(^2P_{3/2})$	$4d^8\,5s\,7s\,(^1G_4)$	$4d^9\,(^2D_{3/2})$	8.77
3	$4p^5 4d^{10}\,5s\,6s\,(^2P_{3/2})$	$4d^8\,5s\,6s\,(^3F_2)$	$4d^9\,(^2D_{3/2})$	1.64
9	$4p^5 4d^{10}\,5s\,6s\,(^2P_{3/2})$	$4d^8\,5s\,6s\,(^1D_2)$	$4d^9\,(^2D_{3/2})$	3.01
10	$4p^5 4d^{10}\,5s\,6s\,(^2P_{3/2})$	$4d^8\,5s\,6s\,(^3G_3)$	$4d^9\,(^2D_{3/2})$	3.16

that the 96 eV peak in Fig. 1 belongs to states of the $4d^7 5s^2$ configuration.

As the $4s^{-1}$ hole has a binding energy of about 115 eV, the kinetic energy of an Auger electron from a $4s^{-1} \rightarrow 4p^{-1}4d^{-1}$ SCK transition involved in the formation of the $4d^7 5s^2$ peak must be in the range $0 \leqslant E_{\rm kin}^{A1} \leqslant 19$ eV. The second Auger electron leading to a tricationic state can be expected to be emitted within a kinetic-energy range given by the difference in binding energies of the accessible $4p^{-1}4d^{-1}$ states discussed above and the final-state binding energy of about 96 eV; this implies a kinetic-energy range of $0 \leqslant E_{\rm kin}^{A1} + E_{\rm kin}^{A2} \leqslant 19$ eV.

As the $4p^{-1}4d^{-1} \rightarrow 4d^{-3}$ GCK decay is expected to be very rapid [23], it is however difficult to distinguish it from a direct $4s^{-1} \rightarrow 4d^{-3}$ double Auger decay. Both direct $4s^{-1} \rightarrow 4d^{-3}$ double Auger decay and the $4s^{-1} \rightarrow 4p^{-1}4d^{-1} \rightarrow 4d^{-3}$ decay channel are further supported by the coincidence map in Fig. 6. This coincidence map presents two Auger electrons emitted in formation of the 96 eV tricationic final-state peak; in this map an energy sharing between the two Auger electrons is observed. Also, the kinetic-energy sum of the first and second Auger electron is approximately 20 eV, which is close to the about 19 eV energy sharing discussed above.

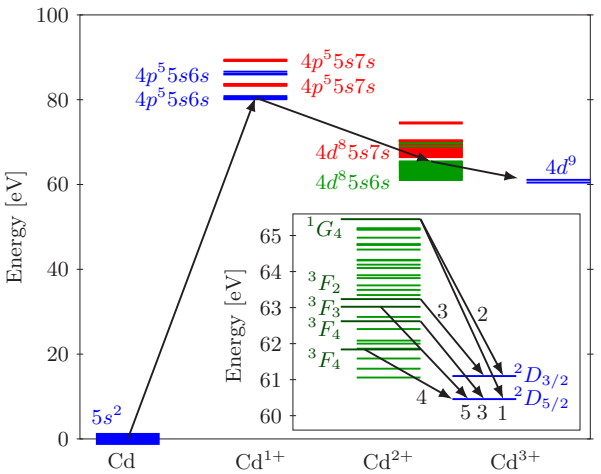

FIG. 5. (Color online) Level diagram illustrating the strongest observed transitions. The numbers included in the inset relate to the peak numbers used in Fig. 4 and Table III.

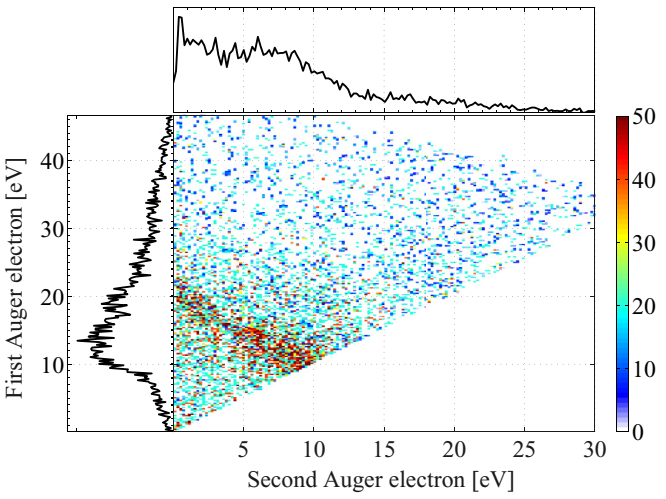

FIG. 6. (Color online) Coincidence map of the first and second Auger electrons associated with the $4d^7 5s^2$ formation. The map reflects a signature of continuous energy sharing between the two Auger electrons with a total energy of approximately 20 eV.

V. CONCLUSIONS

The triple ionization spectrum of atomic Cd involving $4p$ and $4s$ inner-shell vacancies was obtained at 200 eV photon energy using a versatile multielectron coincidence technique. The analysis of the experimental data was supported by multiconfiguration Dirac-Fock calculations. The experimental data revealed a strong selectivity among different possible decay pathways leading to tricationic final states. Our numerical calculations identified the four strongest final-state configurations, suggesting that the channels leading to the observed final-state features all involve a $4p^{-1}$ hole. The decay of the $4p^{-1}$ hole is confirmed to be governed by rapid Coster-Kronig transitions leading to significant spectral broadening in the associated Auger spectra. Also, at the chosen photon energy the ground state of Cd^{3+} was found to be formed primarily by removal of a $4p$ electron. Consequently, as only the first of two Auger transitions involved the $4p^{-1}$ hole, the most prominent last steps of the sequence leading to the Cd^{3+} ground state could be identified in good agreement with our theoretical investigations. The decay of the $4s^{-1}$ hole leading to $4d^7 5s^2$ states was found to involve either two Coster-Kronig transitions, both involving the $4p$ level, leading again to significant broadening in the corresponding Auger spectra, or a direct double Auger decay.

ACKNOWLEDGMENTS

This work has been financially supported by the Swedish Research Council (VR) and the Knut and Alice Wallenberg Foundation, Sweden. We would like to warmly acknowledge the support by the staff and colleagues at the Helmholtz Centre for Materials and Energy GmbH BESSY-II, Berlin. This work was also supported by the European Community–Research Infrastructure Action under the FP6 "Structuring the European Research Area" Programme (through the Integrated Infrastructure Initiative "Integrating Activity on Synchrotron and Free Electron Laser Science," Contract No. R II 3-CT-2004-506008).

[1] K. Siegbahn *et al.*, *ESCA Applied to Free Molecules* (North-Holland, Amsterdam, 1970).
[2] J. H. D. Eland, O. Vieuxmaire, T. Kinugawa, P. Lablanquie, R. I. Hall, and F. Penent, Phys. Rev. Lett. **90**, 053003 (2003).
[3] E. Andersson, P. Linusson, S. Fritzsche, L. Hedin, J. H. D. Eland, L. Karlsson, J. E. Rubensson, and R. Feifel, Phys. Rev. A **85**, 032502 (2012).
[4] P. Linusson, S. Fritzsche, J. H. D. Eland, M. Mucke, and R. Feifel, Phys. Rev. A **87**, 043409 (2013).
[5] P. Linusson, L. Hedin, J. H. D. Eland, R. J. Squibb, M. Mucke, S. Zagorodskikh, L. Karlsson, and R. Feifel, Phys. Rev. A **88**, 022510 (2013).
[6] Y. Hikosaka, P. Lablanquie, F. Penent, T. Kaneyasu, E. Shigemasa, J. H. D. Eland, T. Aoto, and K. Ito, Phys. Rev. A **76**, 032708 (2007).
[7] J. Palaudoux, P. Lablanquie, L. Andric, K. Ito, E. Shigemasa, J. H. D. Eland, V. Jonauskas, S. Kučas, R. Karazija, and F. Penent, Phys. Rev. A **82**, 043419 (2010).
[8] S. P. Kowalczyk, L. Ley, R. L. Martin, F. R. McFeely, and D. A. Shirley, Faraday Discuss. Chem. Soc. **60**, 7 (1975).
[9] U. Gelius, J. Electron. Spectrosc. Relat. Phenom. **5**, 985 (1974).
[10] M. Ohno, Phys. Scr. **21**, 589 (1980).
[11] M. Ohno, J. Phys. C: Solid State Phys. **13**, 447 (1980).
[12] M. Ohno, J. Electron. Spectrosc. Relat. Phenom. **131-132**, 3 (2003).
[13] P. Linusson, S. Fritzsche, J. H. D. Eland, L. Hedin, L. Karlsson, and R. Feifel, Phys. Rev. A **83**, 023424 (2011).
[14] J. F. McGilp and P. Weightman, J. Phys. B **13**, 1953 (1980).
[15] S. Plogmaker, P. Linusson, J. H. D. Eland, N. Baker, E. M. J. Johansson, H. Rensmo, R. Feifel, and H. Siegbahn, Rev. Sci. Instrum. **83**, 013115 (2012).
[16] T. X. Carroll, J. D. Bozek, E. Kukk, V. Myrseth, L. J. Sæthre, T. D. Thomas, and K. Wiesner, J. Electron. Spectrosc. Relat. Phenom. **125**, 127 (2002).
[17] J. H. D. Eland, R. Feifel, and D. Edvardsson, J. Phys. Chem. A **108**, 9721 (2004).
[18] A. Kramida, Yu. Ralchenko, and J. Reader, NIST Atomic Spectra Database. Available at http://physics.nist.gov/asd.
[19] S. Fritzsche, Comput. Phys. Commun. **183**, 1525 (2012).
[20] F. A. Parpia, C. Froese Fischer, and I. P. Grant, Comput. Phys. Commun. **94**, 249 (1996).
[21] J. Olsen, M. R. Godefroid, P. Jönsson, P. Å. Malmqvist, and C. F. Fischer, Phys. Rev. E **52**, 4499 (1995).
[22] A. N. Ryabtsev, R. R. Kildiyarova, and Y. N. Joshi, Phys. Scr. **47**, 59 (1993).
[23] M. Ohno and J.-M. Mariot, J. Phys. C **14**, L1133 (1981).
[24] M. Ohno, J. Electron. Spectrosc. Relat. Phenom. **160**, 15 (2007).